Acta Cryst. (1995). A**51**, 548–558

The Diffraction of X-rays by Close-Packed Polytypic Crystals Containing Single Stacking Faults. III. Measurements of Diffraction Effects Caused by Stacking Faults in Plate or Film Form Samples

BY E. MICHALSKI, W. PIECEK AND M. DEMIANIUK

Institute of Technical Physics, Military Academy of Technology, 00908 *Warsaw, Poland*

(*Received* 8 *June* 1994; *accepted* 3 *February* 1995)

Abstract

A theory that describes the diffraction effects from stacking faults in close-packed polytypic crystal structures was developed in two previous papers of this series [Michalski (1988). *Acta Cryst.* A**44**, 640–649; Michalski, Kaczmarek & Demianiuk (1988). *Acta Cryst.* A**44**, 650–657]. In this paper, attention is paid to the measurement of these diffraction effects for the cases where needle-shaped or rod-like specimens cannot be made from the given sample (*e.g.* thin films) or when single-crystal samples should not be destroyed for preparing such specimens. For this purpose, methods of measurement based on standard X-ray diffraction equipment such as oscillation or Weissenberg cameras and a powder diffraction diffractometer have been developed A complete description of the limitation of the area of the reciprocal lattice that can intersect the Ewald sphere has been provided. Examples of the results obtained by these methods are given. The diffractometer two-dimensional scanning method, which allows an undistorted reciprocal lattice to be recorded and higher precision and results more convenient for mathematical treatment than in photographic methods to be obtained, seems to be especially interesting.

1. Introduction

Results of measurements of diffraction effects caused by stacking faults in different structures were described by, among others, Jagodzinski (1954, 1971), Mitchell (1956), Jagodzinski & Arnold (1960), Rai & Krishna (1968), Jain & Trigunayat (1970), Krishna & Marsall (1971*a*,*b*), Lal & Trigunayat (1971), Steinberger, Kiflawi, Kalman & Mardix (1973), Farkas-Jahnke (1973*a*,*b*), Prasad & Srivastava (1973), Kozielski (1975), Pałosz & Przedmojski (1976), Minagawa (1975, 1977, 1978, 1979), Pandey & Krishna (1977), Pandey, Lele & Krishna (1977), Chand & Trigunayat (1977), Prager (1977), Mehrotra (1978), Demianiuk, Kaczmarek, Michalski & Żmija (1979), Pałosz (1981) and Michalski, Demianiuk, Kaczmarek & Żmija (1979, 1981*a*,*b*, 1982).

These results were usually obtained by X-ray diffraction of needle-shaped or rod-like specimens recorded on photographic films. The diffraction effects caused by stacking faults were also observed in other experiments, some of which are mentioned below.

Comparison of Weissenberg and diffractometer methods for measurement of X-ray diffuse scattering from disordered molecular crystals was described by Welberry & Glazer (1985), X-ray diffraction studies of powder samples of disordered crystals of $A^{II}B^{VI}$ compounds were described by Pałosz & Przedmojski (1978), high-temperature neutron diffraction studies of single-crystal samples of cobalt were described by Frey & Boysen (1981) and results of using high-resolution electron microscopy (HREM) for this study were described by Iijima (1982).

In Berliner, Fajen, Smith & Hitterman (1989), measurement of diffraction effects caused by stacking faults in the $9R(12)_3$ structure was made by low-temperature neutron diffraction of powder samples of Li and Na crystals. The results favourably compared with theory (Michalski, 1988; Michalski, Kaczmarek & Demianiuk, 1988) and computer model analysis (Berliner & Werner, 1986).

Recently, it has become necessary to study stacking faults in crystal structures of thin films or plates in view of new technological possibilities to change the layer arrangement in modern technology [especially the molecular-beam epitaxy (MBE) method], which is used for crystallization of materials with required properties (*e.g.* semimagnetic semiconductors). The influence of some factors on changes in layer arrangement has already been partially examined. For example, the influence of some impurities on the crystal structures of $A^{II}B^{VI}$ compounds was described by, among others, Pałosz & Przedmojski (1976) and Michalski, Demianiuk, Kaczmarek & Żmija (1979, 1981*a*,*b*, 1982).

On the other hand, it is known (Warren, 1959; Verma & Krishna, 1966) that for identification of the layer-arrangement sequence in both the base polytypic structure and regions with faults, it is sufficient to register the X-ray diffraction distribution along small parts of chosen reciprocal-lattice rows. It is not necessary to register the large area of the reciprocal lattice.

ISSN 0108-7673

Therefore, sufficient information about the structure can be obtained without destroyng the samples for the preparation of needle-shaped or rod-like specimens.

2. Area of the reciprocal lattice that can intersect the Ewald sphere for samples in the form of crystal thin films or plates

In planning the measurements for registration of the reciprocal lattice from samples in the form of crystal thin films or plates, it is necessary to take into consideration the consequence of satisfying the conditions $2\theta > \omega$ or $2\theta > (180° - \omega)$, which are connected with the screening of the diffracted beam by the sample, where the angle ω indicates the position of the sample surface (of the specimen holder for the goniometer) in its rotation around the axis of the cameras (or main axis of the goniometer) measured from the direction of the primary beam (for the upper-level Weissenberg equi-inclination method, the reflection angle 2θ is replaced by an angle $2\theta'$, which is the projection of angle 2θ onto the plane of the nth layer). This gives an additional limitation of the area of the reciprocal lattice that can intersect the Ewald sphere. This is illustrated in Fig. 1 for different methods.

In the case presented in Fig. 1(a), not all the points inside the limiting-sphere section [the circle described by the expression $2\lambda^{-1}\exp(i\omega)$; $0 < \omega < 2\pi$] can intersect the Ewald sphere (circle). Only the points lying between one half of the limiting-sphere section [the semicircle described by the expression $2\lambda^{-1}\exp(i\omega)$; $0 < \omega < \pi$] and two halves of the Ewald circles described by the expression $\lambda^{-1}[\exp(i\omega) \pm 1]$, where $-$ corresponds to the

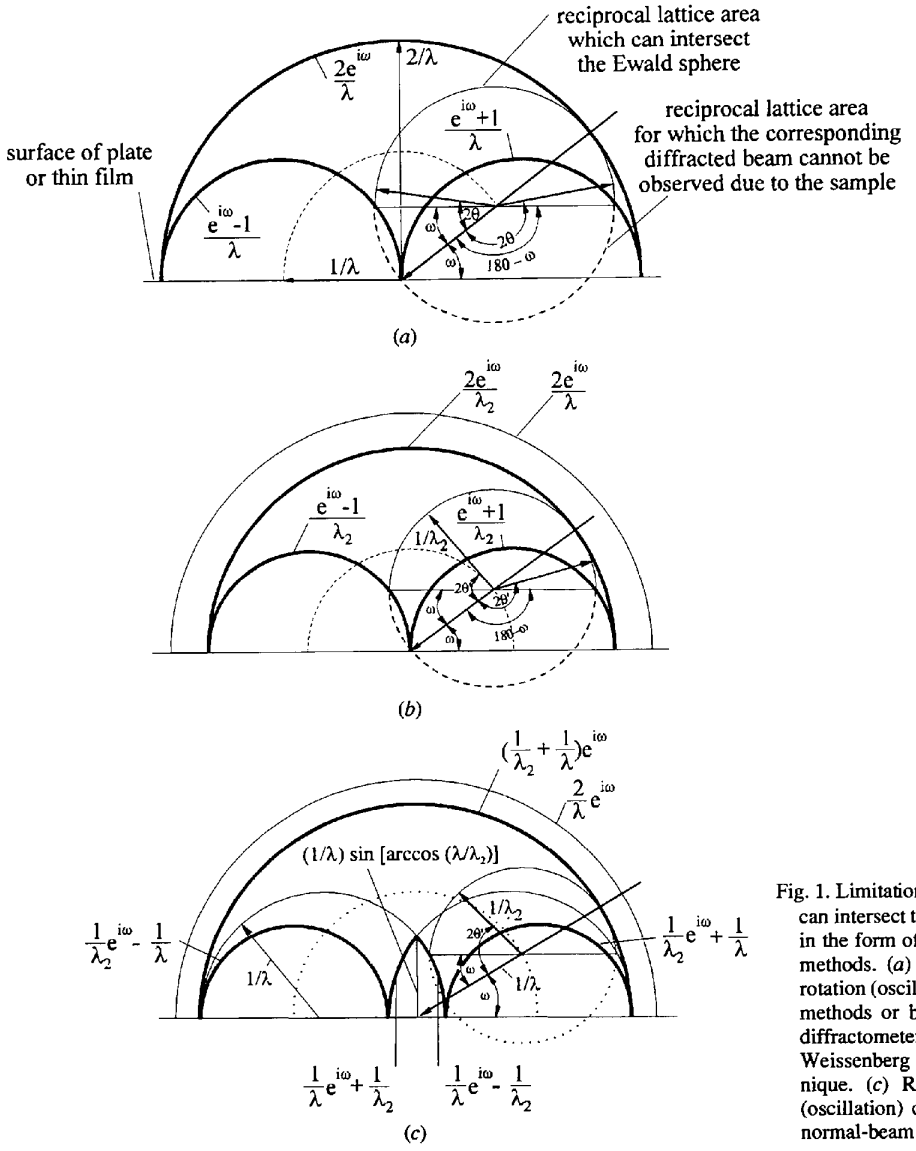

Fig. 1. Limitation of the area of the reciprocal lattice that can intersect the Ewald sphere in the study of samples in the form of crystal thin films or plates by different methods. (a) Recording of the zero-layer plane by rotation (oscillation) of crystal or Weissenberg camera methods or by using a standard powder diffraction diffractometer. (b) Recording of upper layers on Weissenberg camera by the equi-inclination technique. (c) Recording of upper layers on rotation (oscillation) crystal or Weissenberg cameras by the normal-beam method.

condition $2\theta = \omega$ and + to $2\theta = (180° - \omega)$, can intersect.

For recording of the upper layers on the Weissenberg camera by the equi-inclination method, Fig. 1(*b*), the reciprocal-lattice area that can intersect the Ewald sphere is similarly constructed. The only difference is that the radii of both the limiting- and the Ewald-sphere sections are smaller and expressed by the well known expression

$$1/\lambda_2 = [(1/\lambda)^2 - i^2(a_i^*)^2]^{1/2}, \quad (1)$$

where a_i^* is the identity period of the reciprocal lattice along the oscillation axis and i is a Miller index.

In the case presented in Fig. 1(*c*), the Ewald sphere can only intersect the points enclosed between the semicircle described by $(\lambda^{-1} + \lambda_2^{-1})\exp(i\omega)$, $0 < \omega < \pi$, two semicircles described by $\lambda_2^{-1}\exp(i\omega) \pm \lambda^{-1}$, $0 < \omega < \pi$, and two arcs described by $\lambda^{-1}\exp(i\omega) \pm \lambda_2^{-1}$, $0 < \omega < \arccos(\lambda\lambda_2^{-1})$ or $0 < (180° - \omega) < \arccos(\lambda\lambda_2^{-1})$, where − corresponds to the condition $2\theta' = \omega$ and + to the condition $2\theta' = (180° - \omega)$ and $2\theta'$ is the projection of the angle 2θ onto the recorded plane of the reciprocal lattice.

The area that can never intersect the Ewald sphere, enclosed between the arcs described by $\lambda_2^{-1}\exp(i\omega) \pm \lambda^{-1}$, $0 < \omega < \pi$, reaches in the normal plate direction to the points of the reciprocal lattice whose distance from the centre is

$$\lambda^{-1}\sin\arccos(\lambda\lambda_2^{-1}). \quad (2)$$

When the reciprocal-lattice rows parallel to the rotation axis are recorded, the points on these rows are at different distances from the zero-layer plane. The area of the reciprocal-lattice space that can intersect the Ewald sphere depends on this distance. For points positioned on the zero-layer plane, it is the same as in Fig. 1(*a*), whereas for points positioned on the upper-layer plane it is the same as in Fig. 1(*c*).

The construction of the reciprocal-lattice area that can intersect the Ewald sphere presented in Fig. 1 can also be understood analytically. For this purpose, let us equate the modulus of the function $\lambda^{-1}[\exp(i\omega) \pm 1]$ to the length of the diffraction vector $2\lambda^{-1}\sin\theta$:

$$\lambda^{-1}[(\cos\omega \pm 1)^2 + \sin^2\omega]^{1/2} = 2\lambda^{-1}\sin\theta. \quad (3)$$

From (3), we obtain the expected relationships: $2\theta = 180 - \omega$ for + sign and $2\theta = \omega$ for − sign.

The position of the area that can intersect the Ewald sphere on a Weissenberg exposure results from the following expressions (Luger, 1980):

$$y = \theta \quad \text{and} \quad x = g(\alpha + \theta), \quad (4)$$

where $\alpha + \theta = \omega$ and $g = 0.5\,\text{mm}^{\circ-1}$.

As is well known (*e.g.* Luger, 1980), the reciprocal-lattice direction with $\alpha = 0$ (perpendicular to the sample surface) corresponds to the following straight line on the Weissenberg photograph (Fig. 2).

$$x = g\theta = gy \quad (\text{or } x = y/2 \text{ when } g = 0.5). \quad (5)$$

After substituting $\omega = 2\theta$ {corresponding to the curve $\lambda^{-1}[\exp(i\omega) - 1]$} in the equation $\alpha + \theta = \omega$, we obtain $\alpha = +\theta$. This case corresponds to the other straight line in Fig. 2.

$$x = g2\theta = g2y \quad (\text{or } x = y \text{ when } g = 0.5). \quad (6)$$

On the other hand, for curve $\lambda^{-1}[\exp(i\omega) + 1]$ we have $\alpha = -\theta$ and $\omega = 0$. This case corresponds to the straight line $x = 0$.

The aforesaid limitation of the reciprocal-lattice area that can intersect the Ewald sphere is an additional factor to be taken into account in measurements, distinguishing the study of samples in the forms of crystal thin films or plates from the study of rod-like samples.

3. Recording of diffraction effects from stacking faults by the two-dimensional diffractometer scanning method

It is known (Alexander & Smith, 1962; Luger, 1980) that, in diffractometer measurements in the ω–2θ scan mode, the scan is made in the direction of the diffraction vector (reciprocal-lattice vector) while, in the ω-scan mode, it is made in the direction perpendicular to the diffraction vector (reciprocal-lattice vector). Mathieson & Stevenson (1985) have also described a third mode of one-dimensional scanning, which scans the immobile reciprocal lattice along the Ewald circle. For a limited region, adjacent to the point of intersection of this scan direction and diffraction vector, their inclination is equal to θ. According to the notation given by Luger (1980), this scan mode can be denoted by 2θ. Three possible directions of one-dimensional scan mode, described according to the notation given by Luger (1980), are illustrated in Fig. 3. They can be called radial, azimuth and inclined.

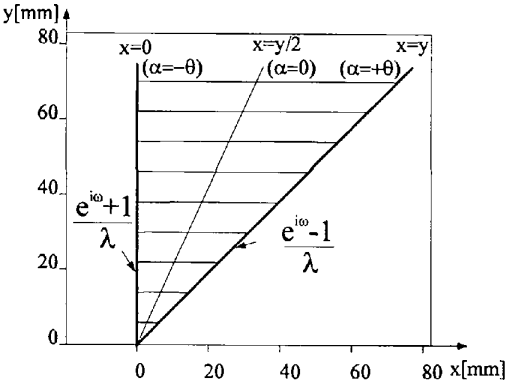

Fig. 2. Position of the reciprocal-lattice area that can intersect the Ewald sphere on a Weissenberg exposure [compare with photographs in Figs. 11(*c*) and 12(*a*)].

It is also known (Warren, 1959; Verma & Krishna, 1966) that the information about the layer arrangement in polytypic structures is contained in the X-ray diffraction distribution along the reciprocal-lattice rows for which $h-k \neq 3r$. These rows in any geometry are not coincident with any directions of one-dimensional scan modes.

Therefore, in our case one-dimensional scan modes are not sufficient. It is necessary to use the method of scanning required for reciprocal-lattice rows inclined to the diffraction vector (reciprocal-lattice vector). For this purpose, the idea of two-dimensional scanning proposed by Mathieson (1982), Mathieson & Stevenson (1984, 1985), Ryan (1992), Wójik (1993), Sass (1993) and Gaca (1993) was applied. The technique of two-dimensional ($\Delta\omega$, $\Delta 2\theta$) scanning first described by Mathieson (1982) and Mathieson & Stevenson (1984) was applied by Mathieson & Stevenson (1985) to the measurement of reflectivity (rocking) curves of imperfect crystals. They also described some properties of two-dimensional space ($\Delta\omega$, $\Delta 2\theta$) in which the results of this scanning were presented.

Wójcik (1993), Sass (1993) and Gaca (1993) applied two-dimensional scanning to the measurement of the satellite reflexions of GaAs(P)/GaAs layered modulated structure. These reflexions were positioned near the point 004 of the reciprocal lattice along the direction almost parallel to its 00l row.

Two examples of such measurements follow. In the first example, the distribution of X-ray diffraction along diffraction vectors is measured (by the ω–2θ-scan mode) for successively settled values of an ω angle (by the sample rotation $\Delta\omega$ alone with immobile counter). Let this method be called the two-dimensional radial scan mode and denoted by the symbol $\Delta\omega$, ω–2θ.

In the second example, the distribution of X-ray diffraction along the arc perpendicular to the diffraction vector (reciprocal-lattice vector) is measured (by the ω-scan mode) for successively settled lengths of the diffraction vector (by movement under the condition $\Delta 2\theta$ equal to $2\Delta\omega$). Let this method be called two-dimensional azimuth scan mode and denoted by $\Delta(\omega$–$2\theta)$, ω.

Both the above-mentioned examples are illustrated in Fig. 4.

In general, there are six possible two-dimensional scan modes: double radial ($\Delta\omega$, ω–2θ and $\Delta 2\theta$, θ–2θ), double azimuth [$\Delta(\omega$–$2\theta)$, ω and $\Delta 2\theta$, ω] and double inclined [$\Delta(\omega$–$2\theta)$, 2θ and $\Delta\omega$, 2θ]. Different factors may affect the choice of one of them. For example, in the first case, fewer $\Delta\omega$ or $\Delta(\omega$–$2\theta)$ steps are sufficient when the inclination between the diffraction vector and the registered row is almost 0°, and in the second case when this inclination is almost 90°.

Determination of ω and 2θ angle ranges for two-dimensional scanning is illustated by examples given below. Let us consider plates of (00.1)- and (10.0)-oriented SiC crystals examined using Cu$K\alpha$ X-ray radiation. The reciprocal-lattice area that can intersect the Ewald sphere for the (00.1)-oriented plate, rotated around the a axis is shown in Fig. 5.

The ω and 2θ angles that satisfy the diffraction condition for the chosen reciprocal-lattice points are determined by the expression

$$\omega_{\pm h0.ln+x} = \theta_{\pm h0.ln+x} + \alpha_{\pm h0.ln+x}, \qquad (7)$$

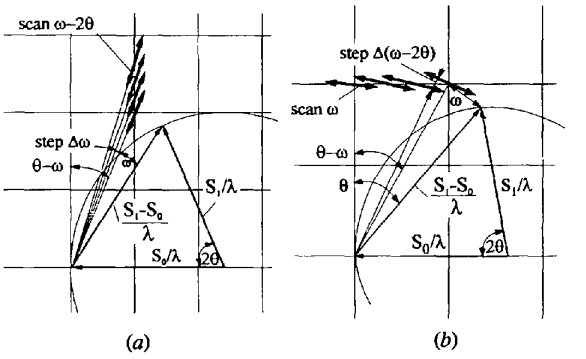

Fig. 4. Illustration of examples of two-dimensional scan modes. (*a*) Radial $\Delta\omega$, ω–2θ, and (*b*) azimuth $\Delta(\omega$–$2\theta)$, ω.

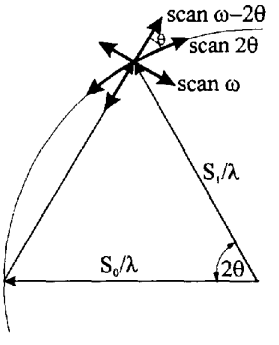

Fig. 3. Directions of three possible one-dimensional scan modes: ω, ω–2θ and 2θ [denoted according to the notation given by Luger (1980)].

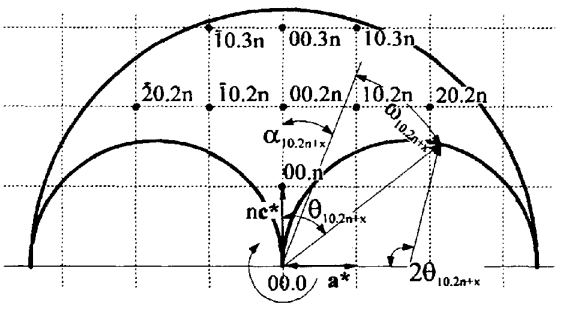

Fig. 5. Illustration of the reciprocal-lattice area that can intersect the Ewald sphere and ω and 2θ angles that satisfy diffraction conditions in the study of (00.1)-oriented plates rotated around the a axis (SiC crystal, Cu$K\alpha$ radiation).

where

$$\theta_{\pm h0.ln+x} = \arcsin(\lambda/2\{(ha^*)^2 + [c^*(l + x/n)]^2\}^{1/2}) \quad (8)$$

$$\alpha_{\pm h0.ln+x} = \arctan\{\pm ha^* n/[c^*(ln + x)]\} \quad (9)$$

and h is the first Miller index, n is the number of layers in a unit cell of a polytype, $(ln + x)$ is the fourth Miller–Bravais index and x can be $1, \ldots, n - 1$.

In the case of thin films or plates of a (10.0)-oriented crystal rotated around the a axis, the reciprocal-lattice area that can intersect the Ewald sphere is illustrated in Fig. 6. The ω and 2θ angles are determined by expressions similar to (7)–(9). Only $\alpha_{\pm h0.ln+x}$ is determined by a different expression:

$$\alpha_{\pm h0.ln+x} = \arctan[(ln + x)c^*/(\pm ha^* n)]. \quad (10)$$

For a diffractometer with independent computer-controlled driving of specimen holder and counter, this measurement can be made in the one-dimensional scan mode using expressions (7)–(10) and substituting the full number of steps instead of n.

After computing, the two-dimensional distribution of X-ray diffraction intensity is drawn as a two-dimensional map. The map can be drawn in $(\Delta\omega, \Delta 2\theta)$ space described by Mathieson & Stevenson (1985) or in polar coordinates [diffraction vector length $2\lambda^{-1}\sin\theta$ and the angle $\alpha = (\theta - \omega)$ of inclination with respect to the surface normal] naturally resulting from measurements. However, for interpretation of the results, the Cartesian coordinates of the reciprocal lattice

$$\begin{aligned} x^* &= (2\sin\theta/\lambda)\sin(\theta - \omega) \\ y^* &= (2\sin\theta/\lambda)\cos(\theta - \omega) \end{aligned} \quad (11)$$

seem to be more convenient. As axis units, one can use Å^{-1} or a multiplier of reciprocal-lattice constants in a given direction. The Jacobi determinant of transformation between reciprocal-lattice space and $\Delta\omega$, $\Delta 2\theta$ space is expressed by

$$\begin{aligned} &2\lambda^{-2}\sin\theta\cos(\theta - \omega)(\cos\omega - \sin\theta) \\ &\times [\cos(\theta - \omega) - \sin(\theta - \omega)]. \end{aligned} \quad (12)$$

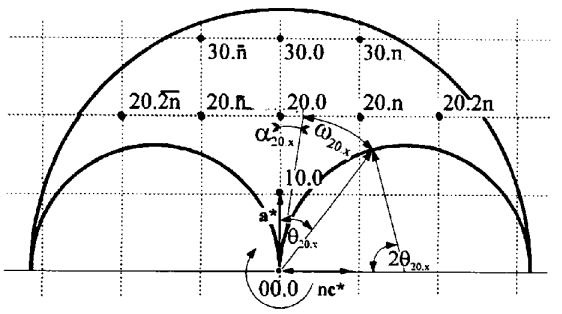

Fig. 6. Illustration of the reciprocal-lattice area that can intersect the Ewald sphere and ω and 2θ angles that satisfy diffraction conditions in the study of (10.0) oriented films or plates by two-dimensional scanning (Cu $K\alpha$ radiation, SiC crystal).

If the radiation $K\alpha$ containing both the α_1 and α_2 components is used in measurements, then the component α_2 has to be removed by one of the known procedures. The components α_2 are shifted from α_1 in the diffraction-vector direction. Therefore, in the case of two-dimensional radial scanning, they can be removed before drawing the maps. In other cases, it has to be done on the basis of the radial sections of maps.

An example of a two-dimensional map of X-ray diffraction intensity distribution along part of row $10.l$ (from $10.2n$ to $10.3n$) for the SiC-$6H(33)$ structure is shown in Fig. 7.

Comparison of the positions of the reciprocal-lattice-point (reflexions) maxima experimentally determined on the basis of the map (obtained with $K\alpha_1$ radiation) for the examined $6H$ structure and calculated for the $6H$ structure without any stacking faults are presented in Table 1. From this comparison, one can see that the maxima of the reciprocal-lattice points (reflexions) 10.13 and 10.17 are shifted about $\Delta h_3(10.13) = +0.00075\ \text{Å}^{-1}$ and $\Delta h_3(10.17) = -0.00060\ \text{Å}^{-1}$ (or in general about $\Delta h_3(6M \pm 1) \simeq 0.00067\ \text{Å}^{-1}$), respectively, in relation to the $6H(33)$ structure without any stacking faults. However, the remaining reciprocal-lattice-point maxima are not shifted.

Using Table 2(*c*) of Michalski, Kaczmarek & Demianiuk (1988), one can easily find that the structure of the examined sample is not the $6H(33)$ structure free from stacking faults and that the faults are not of the same type. Absence of shifts of reflexions $6M \pm 2$ results from the coexistence of stacking faults causing the peak shift of these reflexions in the opposite direction, and of the reflexions $6M \pm 1$ in the same direction (given above). Thus, only the faults described by Zhdanov's symbols [(22), (5), (14), (4) and (211)] can be taken into consideration.

This example illustrates the great potential sensitivity of the above method for studying subtle diffraction effects caused by a very small concentration of stacking faults that are not perceptible by other methods (film methods) in plate or film samples.

4. Registration of diffraction effects from stacking faults in plate or thin-film samples by film methods

4.1. (00.1)-*oriented surface of samples*

Single crystals with a (00.1)-oriented surface are often obtained directly in the crystallization process (*e.g.* SiC crystals) or after cleaving (*e.g.* GaAs and sometimes $A^{II}B^{VI}$ compounds crystals). The influence of dopants on the layer arrangement can be easily observed during crystallization of (00.1)-oriented thin films (*e.g.* by the MBE method).

The structure in the middle (not on the edge) of such oriented surfaces cannot be examined by the *c*-axis crystal oscillation method but can be examined by the Weissenberg method. The choice of oscillation axis

is determined by the condition $h - k \neq 3r$ for the reciprocal-lattice rows to be recorded. When the crystal oscillates around the a axis, sufficient information about the structure is contained in the zero layer of the reciprocal lattice (Fig. 5). When the crystal oscillates around the a axis, diffraction effects of changes in the layer arrangement can be recorded only on the upper layers of the reciprocal lattice.

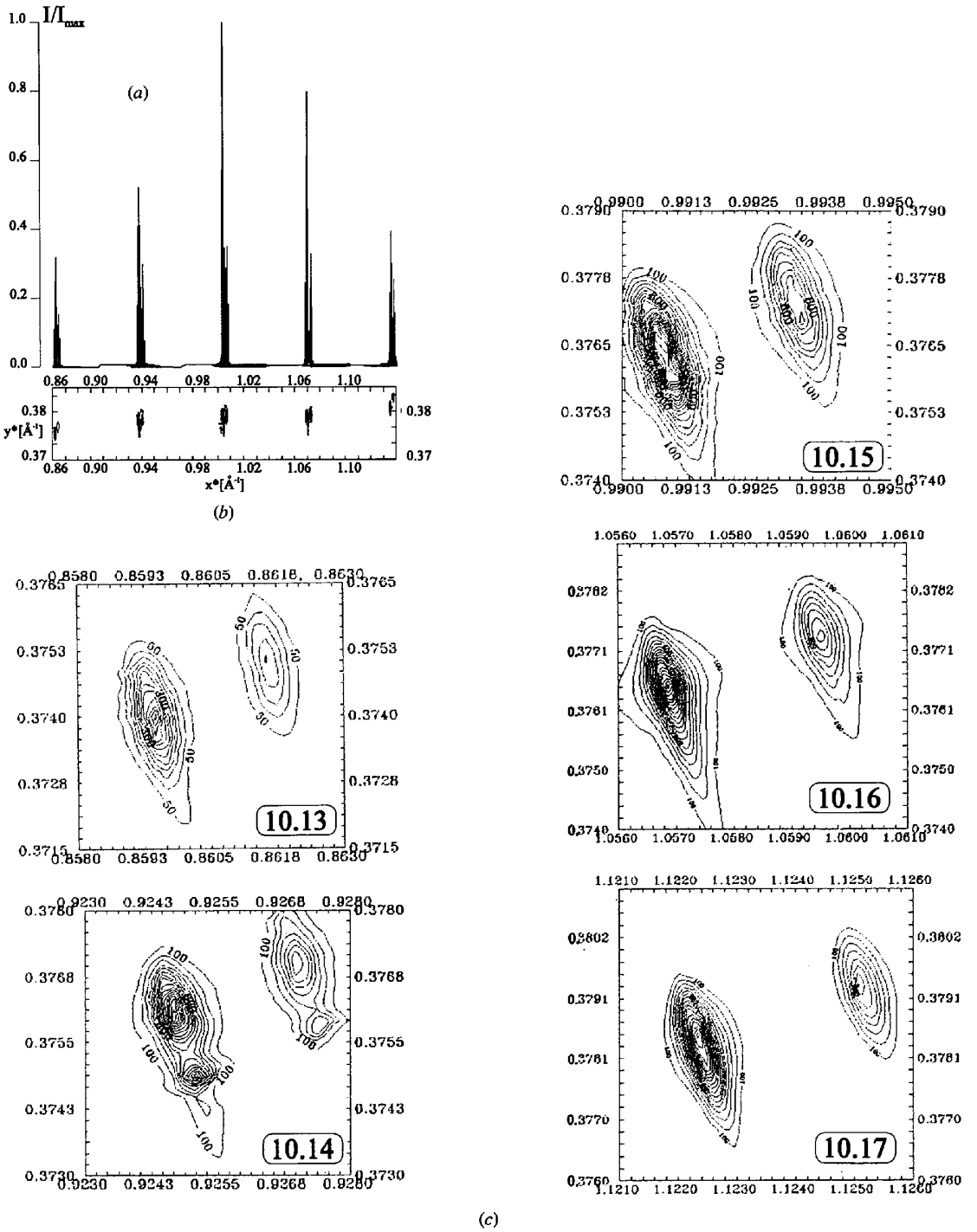

Fig. 7. Experimentally obtained two-dimensional map of X-ray diffraction intensity distribution along part of row 10.l (from 10.2n to 10.3n) for the SiC-6H(33) structure. (*a*), (*b*) Two views of the whole map. (*c*) Particular reflexions magnified (units on axes Å^{-1}, difference of X-ray intensity between neighbouring contour lines corresponds to 100 or 50 counts s^{-1}).

Table 1. *Calculated and observed position of reciprocal-lattice-point maxima for* SiC-6*H* ($Å^{-1}$)

hk.l	10.13	10.14	10.15	10.16	10.17
Structure examined	0.85940	0.92467	0.99075	1.05684	1.12225
Structure without faults	0.85865	0.92470	0.99075	1.05680	1.12285

The area of the reciprocal lattice that can intersect the Ewald sphere for oscillation around the a axis is presented in Fig. 5. Parts of the rows 10.l (from 10.2n to 10.3n), $\bar{1}0.l$ (from $\bar{1}0.2n$ to $\bar{1}0.3n$) and 00.l (00.n, 00.2n and 00.3n), sufficient for layer-arrangement determination, are contained within this area.

Such diffraction geometry has an advantage in relation to the oscillation around the c axis, *viz* by moving the film along the oscillation axis and the crystal parallel to its surface after each exposure, sufficient parts of the reciprocal lattice from many different crystal regions can be recorded on one Weissenberg film, as illustated in Fig. 8. The structure on the surface is changing from $6H(33) + DS$ to $15R(32)_3 + DS$ to $4H + DS$.

4.2. (01.0)-*oriented surface of samples*

Because both c and a axes lie in the (01.0) plane, registration of a sufficient part of the reciprocal lattice is possible with crystal oscillation around the c or a axis. Areas of the zeroth and nth layer of the reciprocal lattice that can intersect the Ewald sphere for oscillation around the c axis are illustated (for SiC crystals) in Fig. 9. Since $a = b$ for a hexagonal crystal, the (01.0) plane is equivalent to the (10.0) plane.

On the basis of Fig. 9 and expressions (1) and (2), one can see that the points of row 10.l on the nth layer of the reciprocal lattice can be recorded only when

$$(1/\lambda)\sin\arccos(1 - \lambda^2 n^2 c^{*2})^{1/2} < a^* \quad \text{(or in equivalent form } nc^* < a^*\text{)}. \tag{13}$$

The condition (13) is satisfied only for the following relation between the lattice constants a and c:

$$c/na > 3^{1/2}/2. \tag{14}$$

Usually for close-packed polytypic crystals these conditions are not satisfied. Thus, the other rows (*e.g.* 20.l and 30.l) must be recorded and larger angles of oscillation are necessary.

For example, in the SiC crystals, the ω angles that satisfy the diffraction condition for 20.0, 20.n, 30.0 and 30.n reflexions are expressed by

$$\omega_{20.0} = \arcsin(\lambda a^*) \tag{15}$$

$$\omega_{20.n} = 90^\circ - \arccos\left[\lambda(4a^{*2} + c^{*2}n^2)/4a^*\right] \tag{16}$$

$$\omega_{30.0} = \arcsin(3\lambda a^*/2) \tag{17}$$

and

$$\omega_{30.n} = 90^\circ - \arccos\left[\lambda(9a^{*2} + c^{*2}n^2)/6a^*\right]. \tag{18}$$

To record sufficient parts of 20.l and 30.l rows, the oscillation range from $\omega_s < \omega_{20.0} = 35.36^\circ$ to $\omega_f > \omega_{30.n} = 77.47^\circ$ is necessary.

4.3. (11.0)-*oriented surface of samples*

The (11.0) crystallographic planes are surfaces of cleavage in many polytypic crystals (*e.g.* in crystals of $A^{II}B^{VI}$ compounds). Thus they often occur in different samples. The a^* and c^* axes lie within the surface but not the a axis. The necessary parts of the reciprocal lattice can be recorded by oscillation around the a^* or c^* axes or around the a axis. However, the diffractometer method of two-dimensional scanning cannot be used in these cases.

From Fig. 10, one can see that for oscillation around the c axis the recording of row 10.l (from zero to n layers) is not possible when $a^* < \lambda^{-1}$, and of row 20.l when $2a^* < \lambda^{-1}$. As these conditions usually prevail, only row 21.l can be recorded.

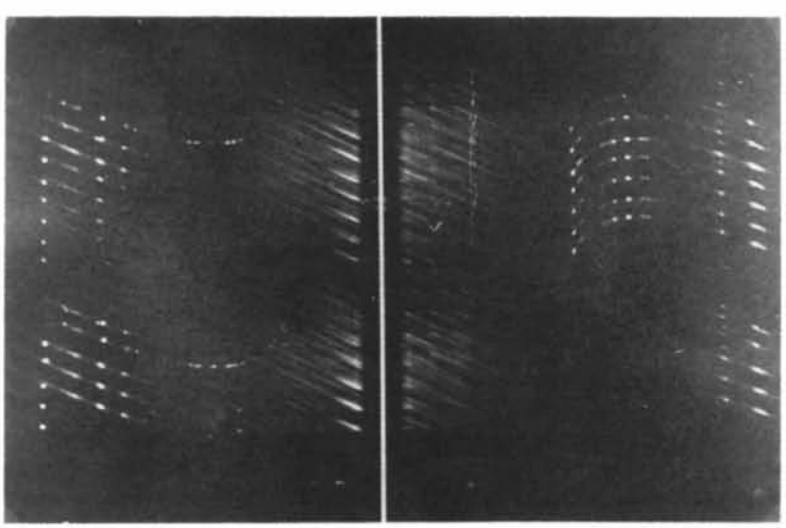

Fig. 8. Parts of rows 10.l registered on a Weissenberg photograph from 12 regions of the (00.1)-oriented surface (SiC crystal, Cu $K\alpha$ radiation, $2r = 5.76$ cm, reduction 1.5×).

The oscillation range necessary for recording the 12.*l* row (from 12.0 to 12.*n*) is determined by the following expressions (Fig. 10*a*):

$$\omega_{12.0} = \arcsin(7^{1/2}\lambda a^*/2) - \arctan(3^{1/2}/9)$$
$$\omega_{12.n} = 90^\circ - \arctan(3^{1/2}/9) - \arccos\left[\lambda(27a^2 + 4n^2c^2)/12(3^{1/2})a^*\right]. \quad (19)$$

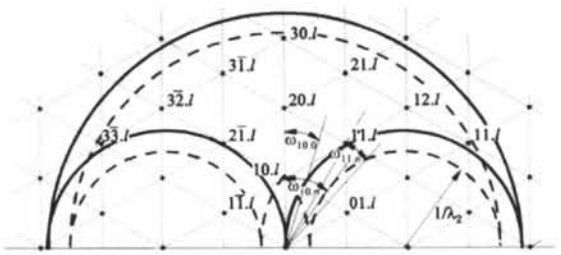

Fig. 9. Areas of the zero layer (continuous line) and the *n* layer (dashed line) of the reciprocal lattice that can intersect the Ewald sphere and angles ω that satisfy the diffraction condition for crystal oscillation around the *c* axis [(10.0)-oriented SiC crystal plate, Cu $K\alpha$ radiation].

For recording the 11.0 and 11.*n* reflections, the following angles must be contained in the oscillation range

$$\omega_{11.0} = \arcsin(3^{1/2}\lambda a^*/2)$$
$$\omega_{11.n} = 90^\circ - \arccos\left[\lambda(3a^* + n^2c^{*2})/2(3^{1/2})a^*\right]. \quad (20)$$

For ZnS crystals and with Cu $K\alpha$ radiation, these angles have value

$$\omega_{12.0} = 27.08, \quad \omega_{12.n} = 33.86, \quad \omega_{11.0} = 23.75, \quad \omega_{11.n} = 33.54^\circ. \quad (21)$$

Therefore, a typical 15° oscillation is sufficient. For preliminary study, the chosen oscillation range can be selected optically, which is more convenient.

In the case of oscillation around the a^* axis, the zero-level Weissenberg exposure does not contain the necessary information about the close-packed layer arrangement. Diffraction effects from stacking faults can only be recorded on the upper-level Weissenberg exposures. Examples are presented in Fig. 11.

The X-ray diffraction photograph presented in Fig. 11(*d*) was obtained by moving the film along the oscillation axis (~ 5 mm) and the crystal parallel to the

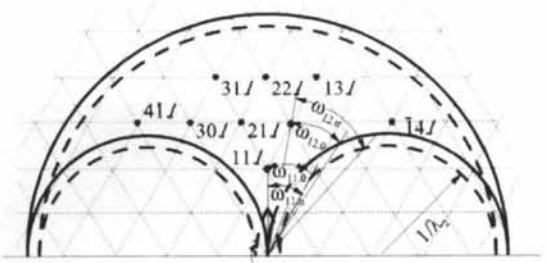

(*a*)

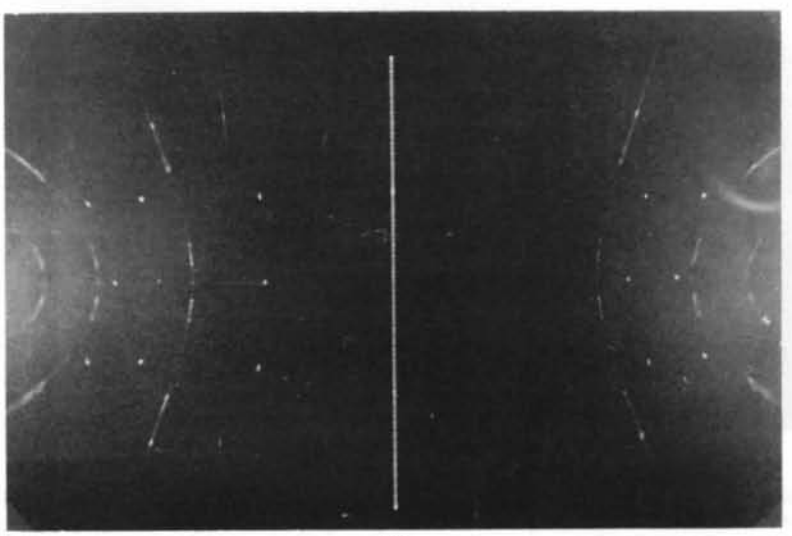

(*b*)

Fig. 10. The case of the *c*-axis-oscillated samples with the (11.0)-oriented surface (ZnS crystal, Cu $K\alpha$ radiation). (*a*) Reciprocal-lattice area that can intersect the Ewald sphere on the zero layer (continuous line) and *n* layer (dashed line), $\lambda_2^{-1} = (\lambda^{-2} - n^2c^{*2})^{1/2}$. (*b*) Photograph ($2r$ = 8.6 cm, reduction 1.5×).

[00.1] direction along its surface (~ 1 mm) after each exposure. The structure of the sample is seen as changing along the [00.1] direction from $4H + DS$ to $12H + DS$ to $6H + DS$.

For taking photographs around the a axis, the sample must be first rotated around $\mathbf{c}^*$ through 30°. Then the diffraction geometry is the same as presented in Fig. 6. Examples of Weissenberg exposures are given in Fig. 12.

It is interesting (see Figs. 6, 11 and 12) that the parts of rows 10.l and 20.l registered during a very small ω angle are diffused in a direction perpendicular to the oscillation axis and exhibit the different structures occurring in the area of surface taken by the X-ray beam. This fact suggests that when the primary-beam section is line-like, the diffraction pattern from all the structures placed on an exposed line along the c axis can be registered during one exposure.

4.4. *Choice of the orientation of samples*

When an orientation of the plate face or thin film is not settled (determined) beforehand by other factors, an analysis of the reciprocal-lattice area that can intersect the Ewald sphere allows one to choose (determine) a suitable orientation to record the desired parts of the reciprocal lattice. For example, in ZnS or SiC crystals with a (11.0)- or (10.0)-oriented surface, the part of row 10.l of the reciprocal lattice from 10.0 to 10.n (see Figs. 9 and 10) cannot be recorded by the c-axis oscillation. It can be recorded after rotating (reorienting) the surface around the c axis through an angle $\omega_1 < \omega < \omega_2$ in

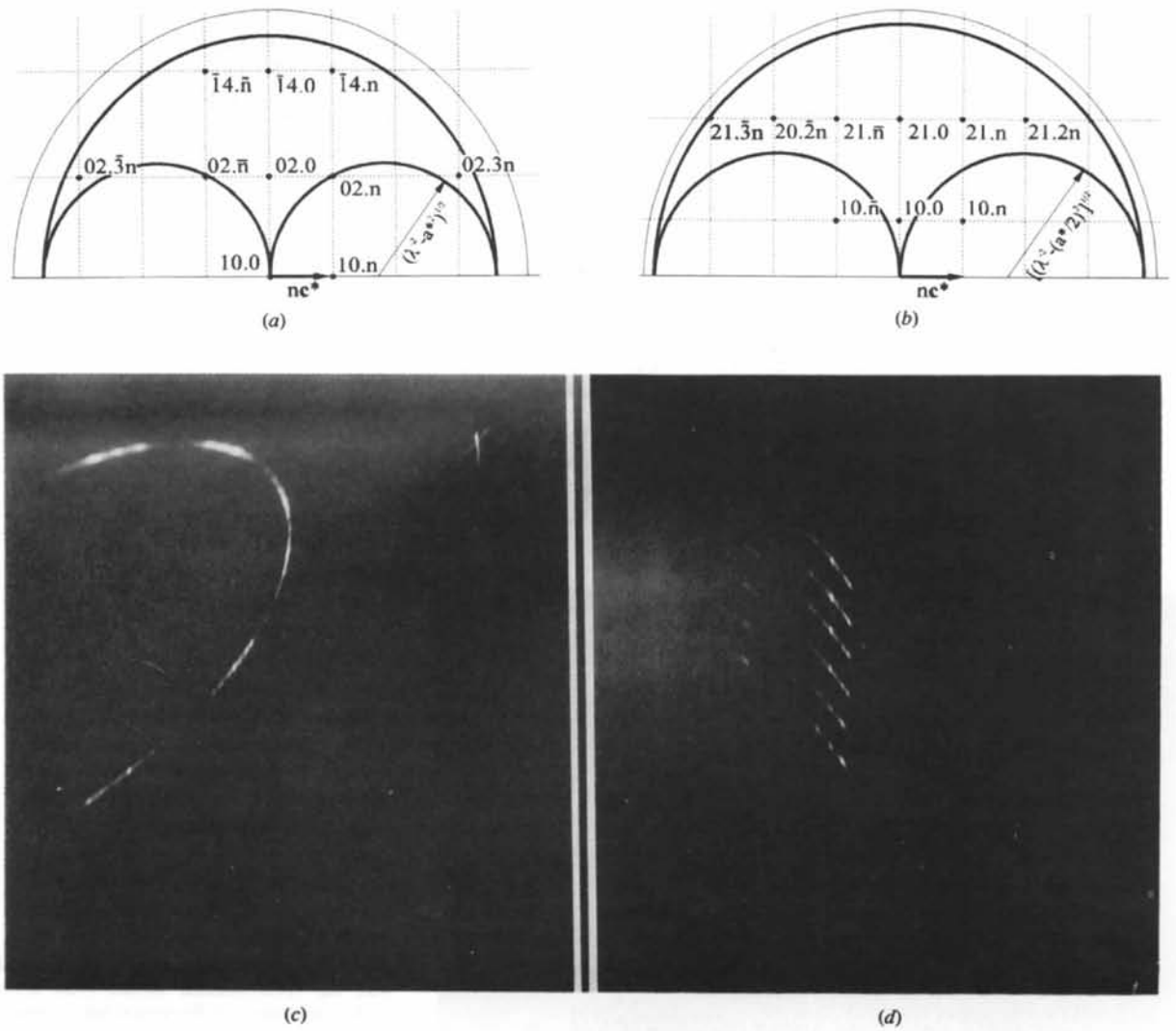

Fig. 11. The case of the a^*-axis-oscillated samples with the (11.0)-oriented surface (upper-level equi-inclination Weissenberg method, ZnS crystal, Cu $K\alpha$ radiation). (*a*), (*b*) Reciprocal-lattice area that can intersect the Ewald sphere. (*c*) X-ray photograph for case (*b*) with the entire area intersecting the Ewald sphere. (*d*) Parts of rows 21.l (from 21.$\bar{n}$ to 21.2$\bar{n}$) from many different regions of the surface ($2r = 5.76$ cm).

relation to the (11.0) plane or through $\omega_3 < \omega < \omega_4$ from the (10.0) plane.

The ω_1 and ω_4 angles mentioned above follow from the limitation of the reciprocal-lattice area that can intersect the Ewald sphere on the zero layer while the ω_2 and ω_3 angles similarly result on an n layer, as follows. From Figs. 9 and 10,

$$\begin{aligned}(a^*/2)\lambda &= \sin(30^\circ - \omega_1)\\ (a^*/2)\lambda &= \sin\omega_4,\end{aligned} \tag{22}$$

which have the solutions

$$\begin{aligned}\omega_1 &= 30^\circ - \arcsin(\lambda a^*/2)\\ \omega_4 &= \arcsin(\lambda a^*/2).\end{aligned} \tag{23}$$

The ω_2 and ω_3 angles concerned with the n layer can be found from the equations

$$\begin{aligned}(1/\lambda)\cos\omega - (1/\lambda_2) &= a^*\cos(\omega_2 + 60^\circ)\\ (1/\lambda)\cos\omega - (1/\lambda_2) &= a^*\cos(90^\circ - \omega_3)\\ (1/\lambda)\sin\omega &= a^*\sin(\omega_2 + 60^\circ)\\ (1/\lambda)\sin\omega &= a^*\cos(90^\circ - \omega_3),\end{aligned} \tag{24}$$

which have the solutions

$$\omega_2 = \arccos\left[(\lambda_2/2a^*)(\lambda^{-2} - \lambda_2^{-2} - a^{*2})\right] - 60^\circ$$

and

$$\omega_2 = 90^\circ - \arccos\left[(\lambda_2/2a^*)(\lambda^{-2} - \lambda_2^{-2} - a^{*2})\right]. \tag{25}$$

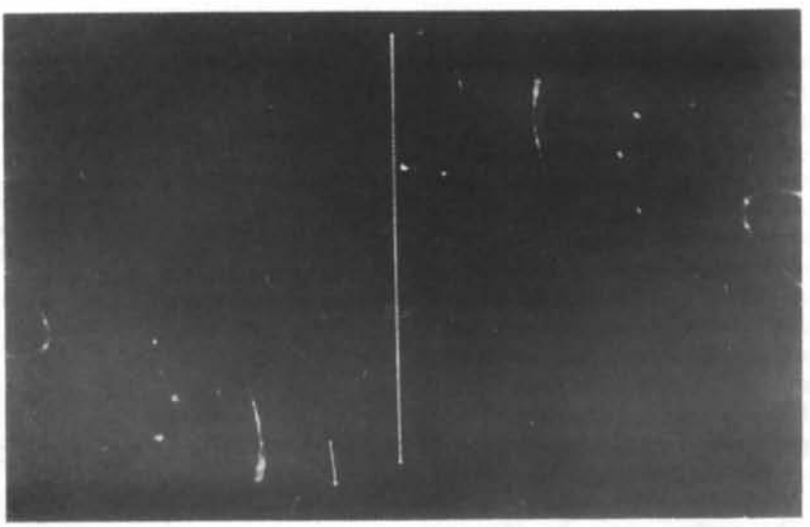

(*a*)

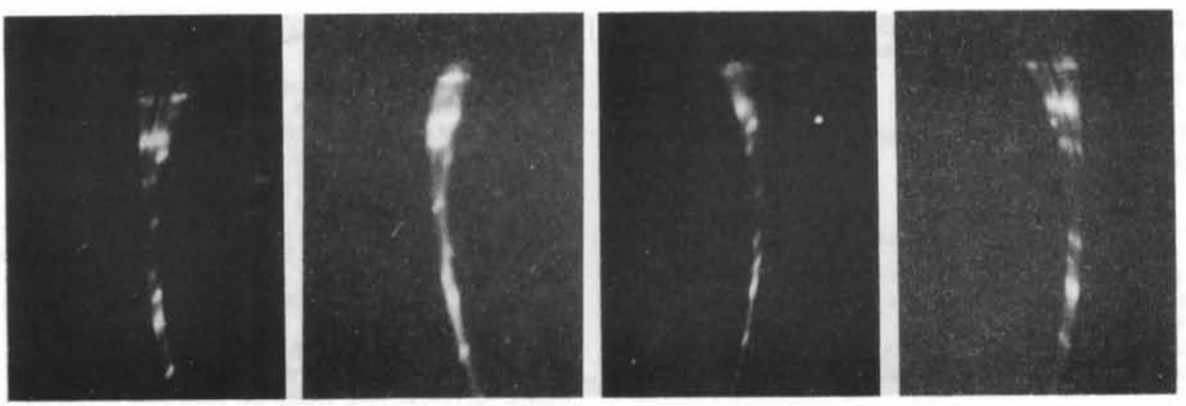

(*b*)

Fig. 12. Parts of rows 10.*l*, 20.*l* and 30.*l* recorded on Weissenberg exposure of the sample with the (11.0)-oriented surface rotated around the c^* axis through 30° (ZnS crystal, Cu $K\alpha$ radiation, $2r = 5.76$ cm). (*a*) Entire reciprocal-lattice area intersecting the Ewald sphere (reduction 1.5×). (*b*) Parts of rows 20.*l* recorded for small ω range (magnification 3×).

Thus the values of these angles are:

for the ZnS crystal,

$$\omega_1 = 16, 55, \omega_2 = 28, 23, \omega_3 = 1, 77, \omega_4 = 13, 45°; \quad (26)$$

for the SiC crystal,

$$\omega_1 = 13.16, \omega_2 = 27.43, \omega_3 = 2.57, \omega_4 = 16.84°. \quad (27)$$

5. Discussion

The method proposed in this paper has some advantages over the methods involving other forms of the specimen. For some cases of examination, only this method is possible. In other cases, it is a more convenient method for primary investigations before specially preparing the specimen. It is also an absolutely non-destructive method.

During the preparation of needle-shaped or rod-like forms of the specimen, some parts of the crystal are always destroyed and so remain unexamined. In the proposed method involving the plate or thin-film form of the samples, there is no such possibility. It is valuable when a succession of structures changing along a given direction in the crystal are examined.

Further, this method seems to be convenient for structural examination during the process of thin-film crystallization. Another advantage is the possibility of obtaining information about the crystal structure in many different crystal regions on a single X-ray film.

Comparing the film and the diffractometer two-dimensional scanning methods, we can see that the latter is not possible for some orientations of the sample surface [*e.g.* (11.0)]. Thus, differently oriented samples become necessary. The method given by Michalski (1994) seems to be convenient for an accurate orientation and setting. The advantages of the diffractometer two-dimensional scanning method are pictures of undistorted reciprocal lattice and greater accuracy and convenience for mathematical treatment.

This work was supported by KBN grant 0819/S2/94/06.

References

ALEXANDER, L. E. & SMITH, G. S. (1962). *Acta Cryst.* **15**, 983–1004.

BERLINER, R., FAJEN, O., SMITH, H. G. & HITTERMAN, R. L. (1989). *Phys. Rev. B*, **40**, 12086–12097.

BERLINER, R. & WERNER, S. A. (1986). *Phys. Rev. B*, **34**, 3586–3603.

CHAND, M. & TRIGUNAYAT, G. C. (1977). *J. Cryst. Growth*, **39**, 299–304.

DEMIANIUK, M., KACZMAREK, S., MICHALSKI, E. & ŻMIJA, J. (1979). *Biul. Wojsk. Akad. Tech.* **28**, 91–97.

FARKAS-JAHNKE, M. (1973*a*). *Acta Cryst.* B**29**, 407–413.

FARKAS-JAHNKE, M. (1973*b*). *Acta Cryst.* B**29**, 413–421.

FREY, F. & BOYSEN, H. (1981). *Acta Cryst.* A**37**, 819–826.

GACA J. (1993). Proc. Liquid and Solid State Crystals: Physics, Technology and Applications, Zakopane, Poland, 1992, pp. 199–202.

IIJIMA, S. (1992). *Acta Cryst.* A**38**, 685–694.

JAGODZINSKI, H. (1954). *Neues Jahrb. Mineral. Monatsh.* **3**, 49–65.

JAGODZINSKI, H. (1971). *Krystallografiya*, **16**, 1235–1246.

JAGODZINSKI, H. & ARNOLD, M. (1960). *Proc. Silicon Carbide Conference, Boston*, 1959, p. 136. New York: Pergamon Press.

JAIN, R. K. & TRIGUNAYAT, G. C. (1970). *Acta Cryst.* A**26**, 463–470.

KOZIELSKI, M. J. (1975). *J. Cryst. Growth*, **30**, 86–92.

KRISHNA, P. & MARSHALL, R. C. (1971*a*). *J. Cryst. Growth*, **9**, 319–320.

KRISHNA, P. & MARSHALL, R. C. (1971*b*). *J. Cryst. Growth*, **11**, 147–150.

LAL, G. & TRIGUNAYAT, G. C. (1971). *J. Cryst. Growth*, **11**, 177–181.

LUGER, P. (1980). *Modern X-ray Analysis on Single Crystals*, pp 59–60, 196–197. Berlin/New York: Walter de Gruyter.

MATHIESON, A. McL. (1982). *Acta Cryst.* A**38**, 378–387.

MATHIESON, A. McL. & STEVENSON, A. W. (1984). *Aust. J. Phys.* **37**, 657–665.

MATHIESON, A. McL. & STEVENSON, A. W. (1985). *Acta Cryst.* A**41**, 290–296.

MEHROTRA, K. (1978). *J. Cryst. Growth*, **44**, 45–49.

MICHALSKI, E. (1988). *Acta Cryst.* A**44**, 640–649.

MICHALSKI, E. (1994). *J. Appl. Cryst.* **27**, 703–709.

MICHALSKI, E., DEMIANIUK, M., KACZMAREK, S. & ŻMIJA, J. (1979). *Acta Phys. Pol.* A**56**, 333–345.

MICHALSKI, E., DEMIANIUK, M., KACZMAREK, S. & ŻMIJA, J. (1981*a*). *Proc. VI Int. Summer School on Lattice Defects in Crystals, Krynica, Poland*, 1980, pp. 300–309. Wrocław: Ossolineum.

MICHALSKI, E., DEMIANIUK, M., KACZMAREK, S. & ŻMIJA, J. (1981*b*). *Acta Phys. Pol.* A**59**, 715–722.

MICHALSKI, E., DEMIANIUK, M., KACZMAREK, S. & ŻMIJA, J. (1982). *Electron Technol.* **13**, 4, 3–8, 9–16.

MICHALSKI, E., KACZMAREK, S. & DEMIANIUK, M. (1988). *Acta Cryst.* A**44**, 650–657.

MINAGAWA, T. (1975). *Acta Cryst.* A**31**, 823–825.

MINAGAWA, T. (1977). *Acta Cryst.* A**33**, 687–689.

MINAGAWA, T. (1978). *J. Appl. Cryst.* **11**, 243–247.

MINAGAWA, T. (1979). *J. Appl. Cryst.* **12**, 57–59.

MITCHELL, R. S. (1956). *Z. Kristallogr.* **103**, 341–355.

PAŁOSZ, B. (1981). *J. Cryst. Growth*, **52**, 969–975.

PAŁOSZ, B. & PRZEDMOJSKI, J. (1976). *Acta Cryst.* A**32**, 409–411, 412–415.

PAŁOSZ, B. & PRZEDMOJSKI, J. (1978). *Acta Cryst.* A**34**, 165–170.

PANDEY, D. & KRISHNA, P. (1977). *J. Cryst. Growth*, **42**, 639–643.

PANDEY, D., LELE, S. & KRISHNA, P. (1977). *J. Cryst. Growth*, **42**, 644–650.

PRAGER, P. R. (1977). *Acta Cryst.* A**33**, 25–28.

PRASAD, B. & SRIVASTAVA, O. N. (1973). *J. Cryst. Growth*, **19**, 11–17.

RAI, K. M. & KRISHNA, P. (1968). *J. Cryst. Growth*, **3**, 741–746.

RYAN, T. W. (1992). Proc. 15th European Crystallographic Meeting, Enschede, The Netherlands, 2–7 August 1992.

SASS, J. (1993). Proc. Liquid and Solid State Crystals: Physics, Technology and Applications, Zakopane, Poland, 1992, pp. 195–198.

STEINBERGER, J. T., KIFLAWI, J., KALMAN, Z. M. & MARDIX, S. (1973). *Philos. Mag.* **27**, 159–175.

VERMA, A. R. & KRISHNA, P. (1966). *Polymorphism and Polytypism in Crystals*. New York: Wiley.

WARREN, B. E. (1959). *Prog. Met. Phys.* **8**, 147–202.

WELBERRY, T. R. & GLAZER, A. M. (1985). *Acta Cryst.* A**41**, 394–399.

WÓJCIK, M. (1993). Proc. Liquid and Solid State Crystals: Physics, Technology and Applications, Zakopane, Poland, 1992, pp. 191–194.